

RAPID CARDIAC MRI USING RANDOM RADIAL TRAJECTORIES

S. M. EL-METWALLY¹, K. Z. ABD-ELMONIEM²,
A. M. YOUSSEF¹ AND Y. M. KADAH¹

ABSTRACT

Using Sparse MRI with random radial trajectories allows MRI images reconstruction from a small number of acquired k -space data. This fulfills the demands of dynamic MRI. Different random radial trajectories are generated by varying the parameters of the added random perturbations to the radial trajectories. Images reconstruction is performed using the non-linear L1 norm reconstruction. Entropy is computed for the reconstructed images, as a quantitative measure for the reconstructed image quality. Both phantom simulation and real cardiac images are used in the experiments of this work. The results show that more sparsely sampled images can be reconstructed with higher quality compared to using non-randomly sampled radial k -space trajectories.

KEYWORDS: Cardiac Magnetic Resonance Imaging (MRI), radial k -space sampling, dynamic imaging.

1. INTRODUCTION

Patient motion during MRI cardiac imaging causes artifacts in the reconstructed image that obscure anatomical details. The main sources of these artifacts are cardiac and respiratory motion. Dynamic MRI captures an object in motion by acquiring a series of images at a high frame rate, thereby reducing motion artifacts. Dynamic imaging places conflicting demands requiring both high spatial resolution to resolve anatomical detail, and high temporal resolution to monitor rapid changes in signal. However, k -space sampling that obeys the Nyquist theorem usually precludes simultaneous achievement of both aims. k -space undersampling speeds up the acquisition by only sampling part of the

required k -space. Sparse MRI is a fast imaging method based on undersampled k -space sampling and non-linear reconstruction [1]. This approach is inspired by theoretical results in sparse signal recovery [2,3]. It has been shown that if the underlying image is compressible it can be recovered from randomly undersampled frequency data, an idea known as compressed sensing. It exploits the fact that medical images often have a sparse representation in some domain “such as finite differences, wavelets, Fourier, etc.”, where the number of coefficients needed to describe the image accurately is significantly smaller than the number of pixels in the image. Uniform undersampling of the Fourier domain results in aliasing. When the undersampling is random, the aliasing is incoherent and acts as additional noise interference in the image representing incoherent interference of the sparse transform coefficients. Sparsity is exploited by constraining the reconstruction to have a sparse representation and to be consistent with the measured k -space data [1]. The success of the reconstruction depends on the sparsity of the coefficients and that the interference is small, having random statistics. This approach has been used with randomly perturbed undersampled spirals [4] and with randomly undersampled 3D Fourier Transform “3DFT” trajectories [5]. It has been shown that the used non-linear L1 norm reconstruction outperformed conventional linear reconstruction, recovering the image even with severe undersampling [4,5].

Radial trajectories have many favorable intrinsic properties with respect to the demands of dynamic MRI including [6]:

- a) Motion-induced artifacts result predominantly in radial streaks with only low intensity near the source of motion and reduce motion-induced ghosting. No ghosts displaced along phase-encoding direction are present.
- b) The coverage of the k -space center in each radial line avoids contrast discontinuities and preserves the continuity of the process. Also, oversampling of the low spatial frequencies provides intrinsic averaging of the gross features of the subject.
- c) By applying a magnitude reconstruction, a reduced sensitivity to statistical phase errors may be achieved, although the amplitude of motion-induced artifacts increases.

¹ Department of Systems and Biomedical Engineering, Cairo University, Cairo, Egypt

² Department of Electrical and Computer Engineering, John Hopkins University, USA

Developing an MR sampling pattern is centered on developing the gradient waveforms, whose integrals traces out a trajectory in the k -space. In current systems, gradients are limited by maximum amplitude and maximum slew rate. Also, physiology provides a fundamental limit to gradient system performance as high gradient amplitudes and rapid switching can produce peripheral nerve stimulation [7]. Random sampling may not be feasible in MR as the k -space trajectories have to be smooth due to these hardware and physiologic considerations. Radial trajectories other than being fast and time-efficient, they result in k -space sampling with a variable density increasing linearly with the inverse of the distance from the k -space origin. Therefore, they are good candidates for random sampling approximation as they are far from being regular as in Cartesian grid sampling despite spanning k -space uniformly [1].

In this paper, we introduce the application of Sparse MRI with random radial trajectories to exploit the intrinsic advantages of these trajectories with respect to the demands of dynamic MRI. Different random radial trajectories are generated by varying the parameters of the added random perturbations to the radial trajectories. Images reconstruction is performed using the non-linear L1 norm reconstruction. Entropy is then computed for the reconstructed images, as a quantitative measure for the reconstructed image quality. The obtained results show that more sparsely sampled images can be reconstructed with higher quality compared to those obtained using uniformly sampled radial k -space trajectories.

The paper is organized as follows: Section two focuses on the methods applied for practical random trajectories generation and image reconstruction. Section three describes the data used in image reconstruction. The results and discussions are included in section four. The conclusions are presented in section five.

2. METHODOLOGY

The block diagram in Fig. 1 summarizes the main applied steps in this work. This section describes these steps in details.

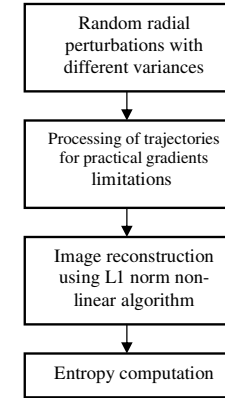


Fig. 1. Block diagram for the main steps employed.

2.1 Random Radial Perturbations

Radial lines are perturbed by slight random deviations taken from Gaussian distribution with zero mean and varying variances. Different schemes for the random perturbations are used in the simulations. These include a) using constant variance along radial lines, and b) using linearly increasing variance with the distance from the k -space origin. i.e., variance is increased in areas of low sampling density and decreased in areas of high sampling density.

Due to the impracticality of pure random sampling of k -space [1], a practical incoherent sampling scheme is aimed to closely mimic the interference properties of pure random undersampling. Therefore, the generated random radial trajectories are processed using a numerical algorithm to keep the gradients amplitude and slew rate below the maximum permissible limits. This algorithm has been used to reshape 2D selective pulses in such a way that one or the other of the applied gradients is always near its maximum allowable amplitude or slew rate, thereby minimizing pulse duration [8]. It involves making discrete steps along the radial trajectory and checking the gradient $g(t) = [g_x(t), g_y(t)]$ and the slew rate $s(t) = [s_x(t), s_y(t)]$ along the way. The i th gradient vectors are expressed as

$$g_i = \frac{\dot{k}(t)}{\gamma} = (1/\gamma\delta t)[k(t_i) - k(t_{i-1})], \quad (1)$$

where, i steps evenly in time, i.e., $t_i = (i-1)\delta t, i = 1, 2, 3, \dots, N$

γ , the gyromagnetic ratio, is set to $4.8 \text{ ms}^{-1} \text{ G}^{-1}$ (or $48 \mu\text{s}^{-1} \text{ T}^{-1}$)

and $\delta t = T/N$ is set to $10 \mu\text{sec}$.

δt is chosen in order to meet practical sampling rates [8].

The discrete slew rate is expressed as the second derivative of k :

$$s_i = \left[1/\gamma(\delta t)^2\right][k(t_i) - 2k(t_{i-1}) + k(t_{i-2})]. \quad (2)$$

The computed gradient and slew rate magnitudes are compared to maximum limits of 0.04T/m and 150T/m/sec (or 4G/cm and 15G/cm/ms) respectively [8]. The k -space coordinates are modified in accordance to satisfy these limitations. The generated random radial trajectory is first processed using a local median filter along each radial line in order to smooth the added variations before applying the practical limits, to preserve the shape of the radially emanating trajectories. Corrections are then made to the smoothed trajectory to satisfy the practical limitations. Figures 2 to 4 show an example for the generated normalized radial k -space trajectories. Figure 2 shows a randomly perturbed radial trajectory using added variance of 3. The trajectory smoothed using the median filter is shown in Fig. 3. The resulting trajectory after corrections to satisfy the practical limitations is shown in Fig. 4.

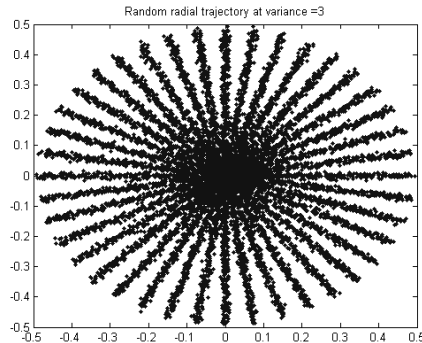


Fig. 2. Randomly-perturbed radial trajectories using added variance of 3.

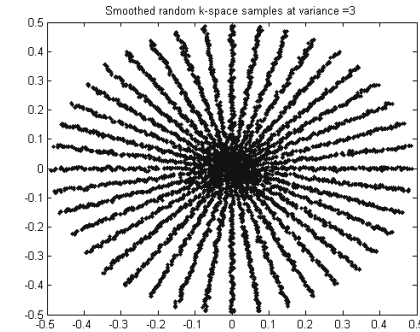


Fig. 3. Randomly-perturbed radial trajectories using added variance of 3 after applying median filter.

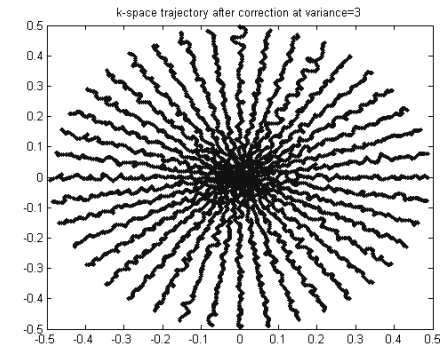


Fig. 4. Randomly-perturbed radial trajectories using added variance of 3 after practical corrections.

2.2 Gridding Reconstruction

In MRI, gridding has been used routinely with respect to nonuniform, non-Cartesian sampling of the k -space [9]. Conventional gridding is applied here to compare with non-linear L1 norm reconstruction using the randomly perturbed radial trajectories. The gridding algorithm is basically performed in four steps:

- a) Precompensate the data with inverse of the sampling density to compensate for the varying density of sampling in k -space. The sampling space is partitioned into several

cells, each cell representing the neighborhood associated with a sample point. The area of each cell is used as the density compensation factor for the corresponding sample point [10].

- b) Convolve with a Kaiser-Bessel window and resample onto a Cartesian grid. A gridding window of width 3 and β parameter of 9 is used.
- c) Apply an inverse two-dimensional Fourier transformation
- d) Postcompensate to remove the apodization of the convolution kernel by dividing by the transform of the Kaiser-Bessel window.

2.3 Non-linear L1 Norm Conjugate- Gradient Reconstruction

Image reconstruction is performed by solving the following constrained optimization problem [1]:

$$\begin{aligned} \min \quad & \lambda \|\Psi(m)\|_1 + \alpha TV(m) \\ \text{s.t.} \quad & \|NFFT(m) - y\|_2 < \varepsilon \end{aligned} \quad (3)$$

where m is the reconstructed image, y is the measured k -space data, Ψ is the sparsifying transform operator, TV or Total-variation is the finite-differences sparsifying transform. Minimizing the objective function promotes sparsity by both the specific transform and finite-differences at the same time. NFFT stands for the Non-uniform Fast Fourier Transform of the image. ε controls the fidelity of the reconstruction to the measured data. The threshold parameter ε is usually set below the expected noise level. α trades Ψ sparsity with finite-differences sparsity. λ is a regularization parameter that determines the trade-off between the data consistency and sparsity.

Equation (3) poses a constrained convex optimization problem. This is converted to the unconstrained problem:

$$\min_m \arg \quad \|NFFT(m) - y\|_2 + \lambda_1 \|\Psi(m)\|_1 + \lambda_2 TV(m), \quad (4)$$

where λ_1 and λ_2 are the weightings of the sparsity and the total variation terms. They represent regularization parameters that determine the trade-off between the data consistency, sparsity and total variation. The values of λ_1 and λ_2 can be determined using trail and error where Eq. (4) is solved for different values, then the values are chosen

such that $\|NFFT(m) - y\|_2 \approx \varepsilon$. An iterative non-linear conjugate gradient descent algorithm with backtracking line search is used, following the work in [1].

2.4 Entropy Minimization

The entropy criterion, E , is defined as [11]:

$$E = - \sum_{j=1}^N \frac{B_j}{B_{ss}} \ln \left[\frac{B_j}{B_{ss}} \right], \quad (5)$$

where N is the number of image pixels and B_j is the modulus of the complex value of the j th image pixel or the pixel brightness. B_{ss} is given by the sum of squared brightness.

$$B_{ss} = \sqrt{\sum_{j=1}^N B_j^2}. \quad (6)$$

When all the image energy is located in a single pixel and the remaining pixels are black, the entropy $E = 0$. When a 128 x 128 image has a uniform brightness, $B_j / B_{ss} = 1/128$ for all the pixels and the entropy $E = 621$. Therefore, entropy minimization favors high contrast. This entropy criterion favors alterations to the data that tend to increase the number of dark pixels. It has been used as a focus criterion to remove motion-induced ghosts and blurring from low intensity regions of the image that would otherwise be dark [11]. Entropy is used here as a measure of the reconstructed image quality. It is computed for the reconstructed images using the non-linear L1 norm reconstruction at the different variances added to the randomly perturbed radial trajectories.

3. EXPERIMENTAL VERIFICATION

3.1 Phantom Simulation

A 2D numerical SheppLogan phantom is used. The phantom image is designed as a linear superposition of elliptical objects, whose FTs are scaled ‘‘jinc’’ functions ($\text{jinc } x = J_1(x)/(2x)$, where J_1 is a first-order Bessel function). k -space samples can thus be evaluated directly, therefore the phantom simulates realistic k -space sampling and truncation.

Phantom image reconstruction is done using both non-linear conjugate-gradient method and the conventional gridding reconstruction. The reconstructed phantom

resolution is 160 x 160. k -space undersampling with 8-fold is used. That is, k -space consists of 20 radial lines. Each line consists of 512 samples. Practically, each radial line is acquired during a Repetition Time “TR” interval, which is relatively long. Therefore, the number of samples per line can be increased, as much as permitted by TR, without any increase in the overall acquisition time. Image reconstruction is done in the sparse finite differences domain using $\lambda_1 = 0$ and $\lambda_2 = 0.05$. This is because the SheppLogan phantom represents a piece-wise constant object, and the TV term measures the finite differences in the reconstructed image. Therefore, minimizing the objective function is equivalent to minimizing the finite differences in the piece-wise constant object.

3.2 MRI Data

Cardiac MRI magnitude images are Fourier transformed at various generated random radial trajectories using non-uniform Fourier transform. Undersampling factors of 8 and 10 are used. k -space consists of 16 radial lines with 512 samples/line in the case of 8-fold acceleration, and consists of 13 radial lines with 512 samples/line in the case of 10-fold acceleration. The reconstructed image resolution is 128 x 128. Random perturbations taken from a Gaussian distribution with zero mean and varying variances are added to the generated radial k -space trajectories. Since medical images often have a sparse representation in the wavelets domain, where the number of coefficients needed to describe the image accurately is significantly smaller than the number of pixels in the image, the parameters used in image reconstruction are $\lambda_1 = 0.002$ and $\lambda_2 = 0.005$. A trail and error strategy is followed for these parameters selection such that $\|NFFT(m) - y\|_2 \approx \varepsilon$. The TV term is included in reconstruction in order to reduce the noise level in the reconstructed images.

3.3 Noise Addition

In order to investigate the performance of the non-linear reconstruction in the presence of noise, noise is added to the noiseless SheppLogan phantom at different noise variances of 0.01, 0.03, 0.05, 0.08, and 0.1 corresponding to Signal-to-Noise Ratios

“SNR” of 24, 15, 11, 8, and 6 dB [12]. At each noise level, images are reconstructed using sparsity weighting $\lambda_1 = 0$ and various TV weightings λ_2 . Different values of λ_2 are tried, and the entropy is computed in each time. The λ_2 value that results in the lowest entropy can then be considered to be the most appropriate for reconstruction at that noise level.

4. RESULTS AND DISCUSSION

The results of simulation phantom reconstruction with 8-fold acceleration are shown in Fig. 5. It can be seen that the small ellipses, as pointed to by the arrows, become more resolved by increasing the variance of the added random deviations. This is also accompanied by an overall decrease in image blurring. Image reconstructed by conventional gridding shows much lower quality, compared to those obtained using non-linear reconstruction. It reveals radial streaks arising due to radial k -space trajectories undersampling. However, these radial streaks disappear gradually with increasing the variance in the reconstructed images using non-linear reconstruction. Table 1 demonstrates the computed entropy of the reconstructed phantom at the different variances used. It can be noticed that entropy value decreases with added variance increase. Linearly-increasing variance shows entropy with slightly higher values compared to constant variance.

Figures 6 and 7 display cardiac image reconstruction using 8-fold and 10-fold accelerations, respectively. It can be seen that the fine image details become clearer with added random perturbations compared to using the standard non-random radial trajectory. Also, as variance increases, more contrast enhancement is noticed. Even at very high undersampling of 10-fold, image reconstruction revealed more improvement. Table 2 demonstrates the computed entropy of the reconstructed images using non-linear reconstruction with random radial perturbations at different variances. It can be seen from the table that the entropy decreases with the increase of variance. Images reconstructed using conventional gridding method show lower quality compared to non-linear reconstruction.

Figures 8-10 show the results obtained at selected SNRs of 24, 11, and 6 dB. At each noise level, the reconstructed images at different TV weightings are shown. Table 3 displays the computed entropy for the reconstructed images using various TV weightings λ_2 at the different noise levels. The lowest entropy obtained is written in bold letters. It can be seen that with increasing noise levels, image reconstruction is enhanced by increasing λ_2 to some limit where the computed entropy is lowest then the reconstructed images become worse and entropy increases again.

Table 1. Entropy computed for phantom simulation with 8-fold acceleration.

Variance (normalized squared spatial frequency m^{-2}/m^{-2})	Entropy
0	188.0157
0.5	179.5162
1	178.2168
2	169.2816
3	164.9984
5	163.9202
Linearly increasing in the range [0-2]	175.5284
Linearly increasing in the range [0-3]	172.6915
Linearly increasing in the range [0-5]	167.0321

Table 2. Entropy computed for cardiac image reconstruction with 8-fold and 10-fold accelerations.

Variance (normalized squared spatial frequency m^{-2}/m^{-2})	Entropy	
	8-fold acceleration	10-fold acceleration
0	184.4865	188.2061
0.5	179.0080	180.7773
1	178.4872	180.2663
2	177.7178	179.9855
3	177.2462	179.2541
5	176.8527	179.1331
8	176.3213	178.1366

Table 3. Entropy computed for phantom image reconstruction at different noise levels using various TV weights TV weights (λ_2)

	0.01	0.05	0.08	0.1
24	166.1648	168.6608	171.4463	174.0649
15	176.4939	172.0308	174.1376	175.6731
11	186.0366	179.1503	177.9645	179.9497
8	199.8878	191.1116	189.1271	188.5640
6	207.9811	199.3539	195.7312	194.3866

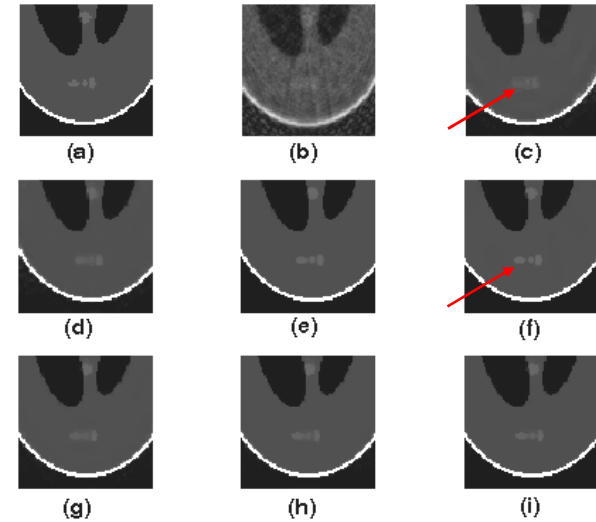


Fig. 5. Phantom image reconstruction with 8-fold acceleration. (a) Original image.

(b) Image reconstructed using conventional gridding. Non-linear conjugate gradient reconstruction using (c) non-random radial k -space, random radial k -space with (d) variance=1, (e) variance=3, (f) variance=5, (g) linearly increasing variance in the range [0-2], (h) linearly increasing variance in the range [0-3], (i) linearly increasing variance in the range [0-5].

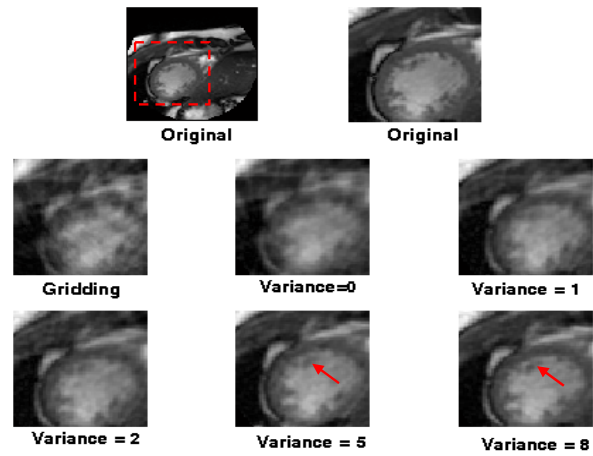


Fig. 6. Enlarged view for the region surrounded by the dashed rectangle showing original and reconstructed cardiac images at 8-fold acceleration. The heart muscles as pointed to by the arrows become more apparent at higher variances.

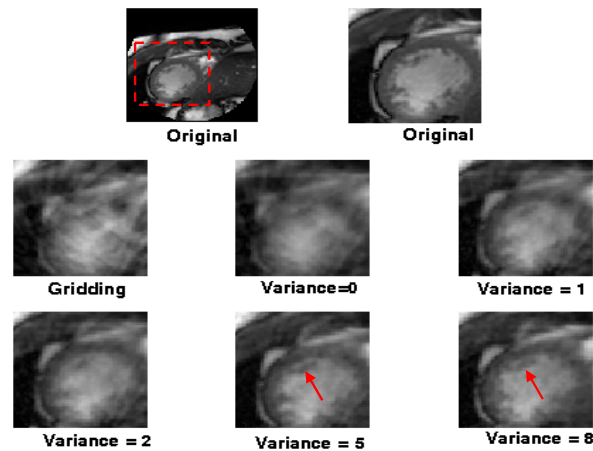


Fig. 7. Enlarged view for the region surrounded by the dashed rectangle showing original and reconstructed cardiac images at 10-fold acceleration.

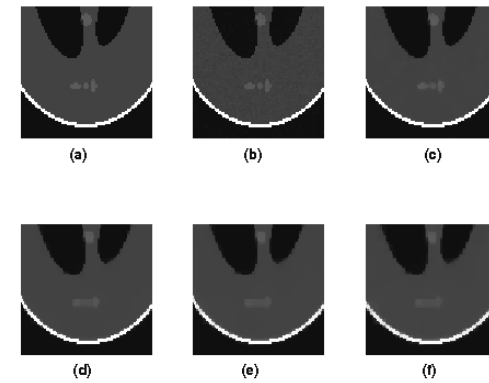


Fig. 8. Phantom image reconstruction at SNR = 24 dB. (a) Original image. (b) Noisy image. Non-linear conjugate gradient reconstruction using (c) $\lambda_2 = 0.01$, (d) $\lambda_2 = 0.05$, (e) $\lambda_2 = 0.08$, (f) $\lambda_2 = 0.1$

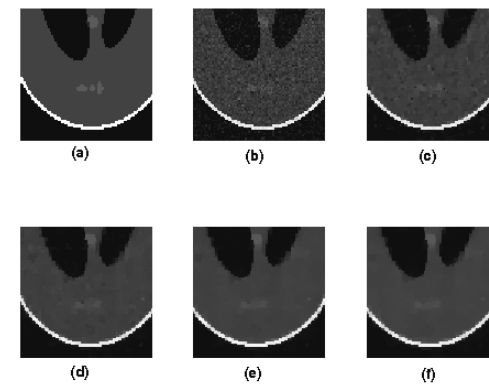


Fig. 9. Phantom image reconstruction at SNR = 11 dB. (a) Original image. (b) Noisy image. Non-linear conjugate gradient reconstruction using (c) $\lambda_2 = 0.01$, (d) $\lambda_2 = 0.05$, (e) $\lambda_2 = 0.08$, (f) $\lambda_2 = 0.1$

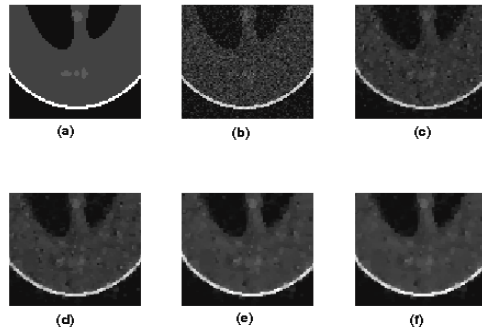


Fig. 10. Phantom image reconstruction at SNR = 6 dB. (a) Original image. (b) Noisy image. Non-linear conjugate gradient reconstruction using (c) $\lambda_2 = 0.01$, (d) $\lambda_2 = 0.05$, (e) $\lambda_2 = 0.08$, (f) $\lambda_2 = 0.1$

5. CONCLUSIONS

In this paper, the concept of compressed sensing is applied in MRI image reconstruction using randomly perturbed radial k -space trajectories. The effect of increasing the variance of the added random components has been investigated for image reconstruction at different undersampling factors or accelerations. The obtained results have shown that using randomly perturbed radial k -space enables more sparsely sampled image reconstruction with higher quality compared to using non-randomly sampled radial k -space trajectories. Also, image reconstruction at high undersampling rates is enhanced by increasing the variance of added random perturbations. The future research should include the investigation of using sparsity transform in non-linear reconstruction of radially sampled images. Also, a study of varying the non-linear reconstruction parameters may be done for different image models such as piece-wise varying and smoothly varying models.

REFERENCES

1. Lustig, M., Donoho, D., and Pauly, J., "Sparse MRI: The Application of Compressed Sensing for rapid MR Imaging", *Magnetic Resonance in Medicine*, Vol. 58, Issue 6, pp. 1182-1195, 2007.

2. Candès, E., Romberg, J. and Tao, T., "Robust Uncertainty Principles: Exact Signal Reconstruction from Highly Incomplete Frequency Information", *IEEE Transactions on Information Theory*, Vol. 52, No. 2, pp. 489-509, 2006.
3. Donoho, D., "Compressed Sensing", *IEEE Transactions on Information Theory*, Vol. 52, No. 4, pp. 1289-1306, 2006.
4. Lustig, M., Lee, J., Donoho, D. and Pauly, J., "Faster Imaging with Randomly Perturbed Undersampled Spirals and L1 Reconstruction", *Proceedings of the ISMRM*, Miami Beach, Florida, USA, 2005.
5. Lustig, M., Donoho, D. and Pauly, J., "Rapid MR Imaging with Compressed Sensing and Randomly Undersampled 3DFT Trajectories", *Proceedings of the ISMRM*, Seattle, Washington, USA, 2006.
6. Rasche, V., De Boer, R., Holz, D. and Proksa, R., "Continuous Radial Data Acquisition for Dynamic MRI", *Magnetic Resonance in Medicine*, Vol. 34, pp. 754-761, 1995.
7. Wright G., "Magnetic resonance imaging", *IEEE Signal Processing Magazine*, Vol. 14, No. 1, pp. 56-66, 1997.
8. Hardy, C. and Cline, H., "Broadband Nuclear Magnetic Resonance Pulses with Two-dimensional Spatial Selectivity", *Journal of Applied Physics*, Vol. 66, No. 4, pp. 1513-1516, 1989.
9. Jackson, J., Meyer, C., Nishimura, D. and Macovski, A., "Selection of a Convolution Function for Fourier Inversion Using Gridding", *IEEE Transactions on Medical Imaging*, Vol. 10, No. 3, pp. 473-478, 1991.
10. Takahashi, A. M., "Consideration for using the Voronoi areas as a k -space weighting function", *Proceedings of the ISMRM*, 7th Annual Meeting, 1999.
11. Atkinson, D., Hill, D., Stoye, P., Summers, P. and Keevil, S., "Automatic Correction of Motion Artifacts in Magnetic Resonance Images Using an Entropy Focus Criterion", *IEEE Transactions on Medical imaging*, Vol. 16, No. 2, pp. 903-910, 1997.
12. Gamper, U., Boesinger, P., and Kozerke, S., "Compressed Sensing in Dynamic MRI", *Magnetic Resonance in Medicine*, Vol. 59, pp. 365-373, 2008.

التصوير السريع للقلب بالرنين المغناطيسي باستخدام المسارات القطرية العشوائية

يقدم البحث تطبيقاً للتصوير بالرنين المغناطيسي باستخدام جزء صغير من القياسات في فضاء التردد المكاني القطري، وبذلك تعد هذه الطريقة مناسبة لإستخدامها في تطبيقات تصوير الأجزاء المتحركة مثل القلب. تعتمد على إحداث تغيرات عشوائية صغيرة على مسارات القياس القطرية ثم إسترجاع الصور باستخدام طرق عددية غير خطية ويقدم البحث نتائج باستخدام نموذج رقمي وصور حقيقية للقلب تظهر أن الصور التي تم إسترجاعها باستخدام المسارات العشوائية أفضل من تلك المستتجة باستخدام المسارات الغير عشوائية.